ceramics

MDPI

Article

Roughness Effect in Micropitting and Rolling Contact Fatigue of Silicon Nitride

Mohsen Mosleh [1], Keron K. Bradshaw [1], Sonya T. Smith [1], John H. Belk [2] and Khosro A. Shirvani [3,*]

1 Department of Mechanical Engineering, Howard University, Washington, DC 20059, USA; mmosleh@howard.edu (M.M.); kkbradshaw@gmail.com (K.K.B.); ssmith@howard.edu (S.T.S.)
2 Zero Technology LLC, Blue Ridge, GA 30513, USA; jhbelk@gmail.com
3 Department of Mechanical Engineering, Rowan University, Glassboro, NJ 08028, USA
* Correspondence: Khosro.A.Shirvani@gmail.com; Tel.: +1-202-746-9766

Received: 31 December 2018; Accepted: 13 February 2019; Published: 18 February 2019

Abstract: An experimental analysis of the role of surface roughness parameters on micropitting and the succeeding rolling contact fatigue (RCF) of silicon nitride against AISI 52100 steel under lubricated conditions was performed. In accelerated fatigue tests using a four-ball tester, the arithmetic mean, root mean square, and peak-to-valley roughnesses of silicon nitride surfaces varied, while the roughness of the steel surface was unchanged. The correlation between the fatigue life and roughness parameters for silicon nitride was obtained. The peak-to-valley roughness was the roughness parameter that dominantly affected the RCF life of silicon nitride. The micropitting of surfaces leading to fatigue intensified as the roughness was increased. Extensive micropitting was observed on the rolling track beyond the trailing edge of the spall region in the circumferential direction.

Keywords: roughness parameters; silicon nitride; peak-to-valley roughness; fatigue; micropitting

1. Introduction

Silicon nitride has been studied as a candidate bearing material for satisfying extreme speed and loading conditions in aerospace and energy applications. The low density, high thermal stability, corrosion resistance, and high hardness of silicon nitride (Si_3N_4) is critical for achieving high DN values (bearing bore diameter multiplied by the rotational speed) in emerging hybrid bearing applications [1]. Advanced manufacturing processes, such as hot isostatic pressing (HIP), permit almost impurity-free densification and produce silicon nitride with a density that approaches the theoretical value that results in good fracture toughness and surface hardness [2,3]. High quality Si_3N_4 rolling elements produced by HIP have also exhibited a rolling contact fatigue (RCF) life that is several times longer than that of steel and fail in non-catastrophic fatigue spalling or delamination modes [4]. The RCF in concentrated contacts, such as rolling bearings, is either near-surface-initiated or subsurface-initiated [5]. In the near-surface-initiated RCF, the surface roughness has a profound effect on the fatigue life—especially at low lambda (λ), which is the ratio of film thickness to composite surface roughness [6,7]. Various parameters, such as arithmetic mean roughness R_a, root mean square roughness R_q, maximum valley depth R_v, maximum peak height R_p, and peak-to-valley roughness R_z, are commonly used to describe the amplitude characteristics of the surface topography and asperities. However, some of the roughness parameters, such as R_a and R_q, which are widely used in various engineering applications, contain averaged-out information on local surface features that potentially affect the RCF life [8]. The RCF studies on ceramic/ceramic material combinations have shown that amplitude roughness parameters related to the valley depth are important in fatigue life [9,10]. The significance of a new roughness parameter, "valley sharpness R_s", which showed

a better correlation with the rolling contact fatigue performance of silicon nitride, is highlighted in another investigation [11]. Considering the significantly higher hardness of silicon nitride compared to steel in hybrid ceramic/steel bearings, its surface roughness takes the dominant role in surface interactions at low lambda (λ), where asperity contact occurs. Therefore, the relationship between the surface roughness of silicon nitride and the RCF life of the hybrid system is of great importance.

Under the continuous cyclic loading in rolling contact situations, fatigue can be initiated from the boundaries of micropitted areas [12,13]. Therefore, factors affecting micropitting in silicon nitride can also affect the RCF life. Experimental studies suggest that a rougher surface is more prone to micropitting and that surface-initiated cracks originate in asperities [14,15]. The initiation and growth of microcracks at notch-like microvalleys, which were oriented favorably against the sliding condition, were shown to produce micropits in gears [16]. Therefore, it has been suggested that superfinishing of gear flank surfaces resists the initiation of micropitting [14]. The polishing process for producing silicon nitride rolling elements is time-consuming and accounts for up to half of the total manufacturing cost. In addition, the idea of obtaining the highest degree of surface polishing with best possible roughness may lead to overengineering of ceramic rolling elements [17]. Various finishing processes, such as conventional lapping and polishing [18], chemical–mechanical polishing [19], magnetic float polishing (MFP) [20], and tribochemical polishing [21], have been utilized to finish silicon nitride and other ceramic rolling elements. Owing to the limitations and characteristics of each polishing process, the resultant roughness parameter that has a dominant role on the RCF life of silicon nitride and other ceramics can be controlled.

In this paper, the impact of arithmetic mean roughness R_a, root mean square roughness R_q, and peak-to-valley roughness R_z on micropitting and the RCF life of silicon nitride when rolling against AISI 52100 steel are investigated. Based on the experimental results, the roughness parameter that dominantly correlates to the RCF life of silicon nitride is presented.

2. Materials and Methods

2.1. Materials and Surface Conditions

The original silicon nitride balls were grade 5 Toshiba TSN-03H ball blanks. Steel balls were made from grade 10 AISI 52100 steel. The race in which the steel balls were rotated was also made from AISI 52100 steel. Material specifications are provided in Table 1. The lubricant was Mobil SHC 626 with a viscosity of 66 cSt at 40 °C, measured per ASTM D 445.

Table 1. Material properties of Si_3N_4 and AISI 52100 steel balls.

Properties	AISI 52100	Silicon Nitride
Hardness (R_c)	60–67	76–80
Diameter (mm)	12.7	12.7
Modulus (GPa)	210	310
Poisson's ratio	0.3	0.26
Density (g/cm^3)	7.81	3.27

The silicon nitride balls were then polished in the laboratory to various surface finishes. The process involved polishing a group of samples from five different sets that were then examined by non-contact profilometry for characterization. The surface profiles and the corresponding surface roughnesses of samples were obtained with the Universal 3D profilometer from Rtec Instrument Inc. The results are presented in Table 2 and the surface images are shown in Figure 1. Due to the spherical shape of the surfaces, the global bow removal feature of the Universal 3D profilometer's software was utilized to obtain the images in Figure 1. The measured R_a roughness of AISI 52100 steel balls was 35 nm in all tests.

Table 2. Roughness characteristics of Si_3N_4 balls.

Sample ID	Diameter (mm)	R_z (μm)	R_a (μm)	R_q (μm)
A (original finish)	12.7	0.312	0.030	0.039
B	12.7	0.388	0.026	0.033
C	12.7	0.961	0.052	0.074
D	12.7	1.259	0.043	0.068
E	12.7	1.578	0.117	0.148
F	12.7	3.720	0.356	0.452

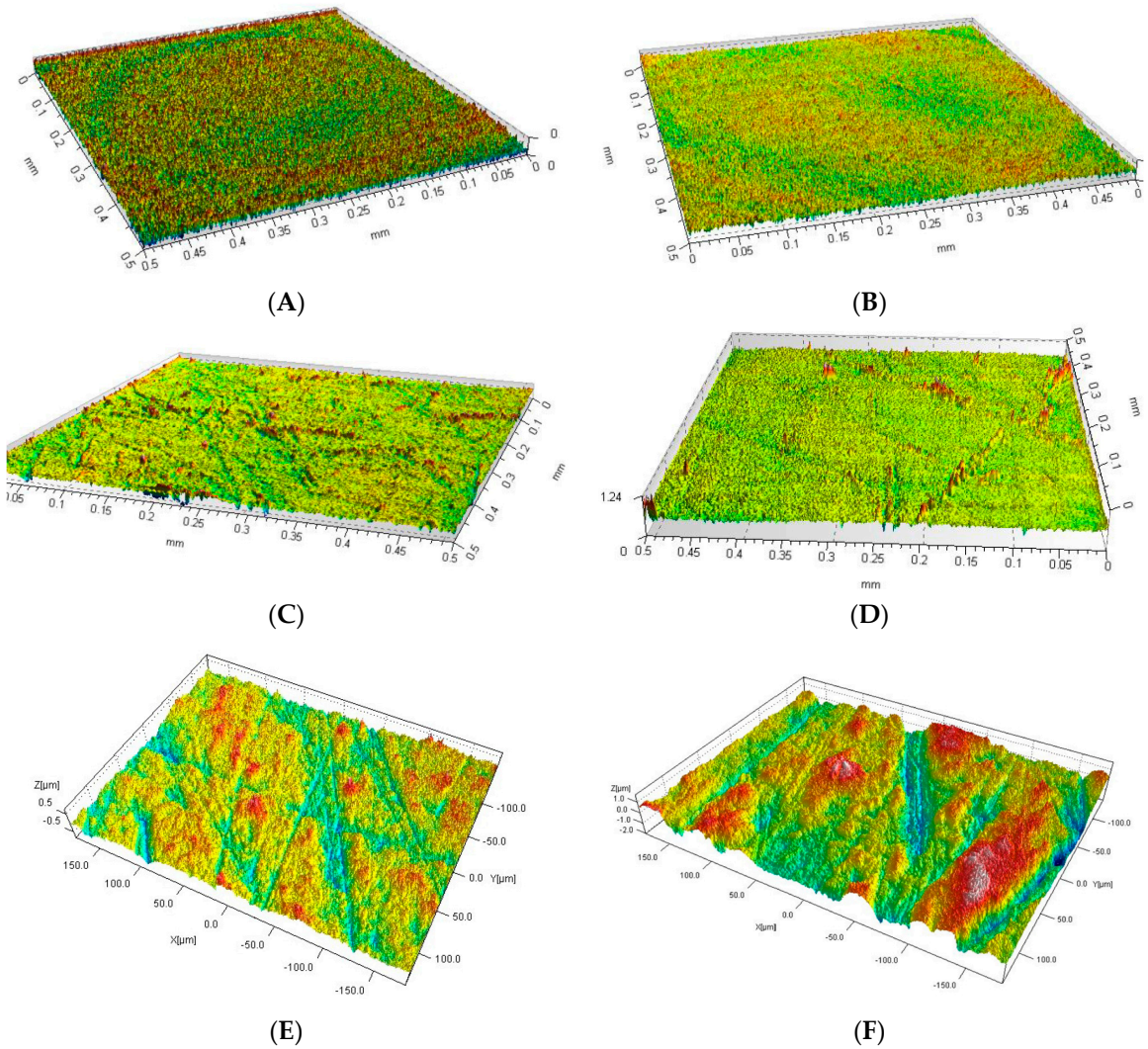

Figure 1. Surface profile of silicon nitride balls with various roughness obtained by non-contact profilometry. Roughness characteristics of surfaces (**A**), (**B**), (**C**), (**D**), (**E**) and (**F**) are shown in Table 2.

2.2. Tester and Test Procedure

A modified Koehler Inc. four-ball tester—capable of operating at 10,000 rpm maximum rotating speed and 10,000 N maximum normal load—was used to conduct the accelerated RCF tests. The ball configuration and geometry are shown in Figure 2. A single-ended compression (SEC)-type piezoelectric accelerometer was used to detect vibration during the RCF tests. Vibrations exceeding a set level indicated the surface fatigue associated with the formation of the first large spall on the surface and resulted in automatic shutdown of the tester. The set vibration level was chosen based on the results at the onset of spalling in silicon nitride balls in pilot RCF tests. A gravity-fed lubrication

supply system with suction return ensured that contacts were lubricated and return oil was filtered before re-entering the supply reservoir. Inline filters were used to prevent wear particles or other particles from entering the supply tank. Also, a 150 W Proportional Integral Derivative (PID)-controlled heater and sensing thermocouple allowed control of the test temperature to be maintained. The initial test temperature was set to 50 °C, which was kept constant during tests. The combination of the PID-controlled heater and the lubricant circulation allowed for a constant test temperature despite frictional heating at the points of contact. A data acquisition system collected data on the operating temperature, rotational speed, normal load, and frictional torque.

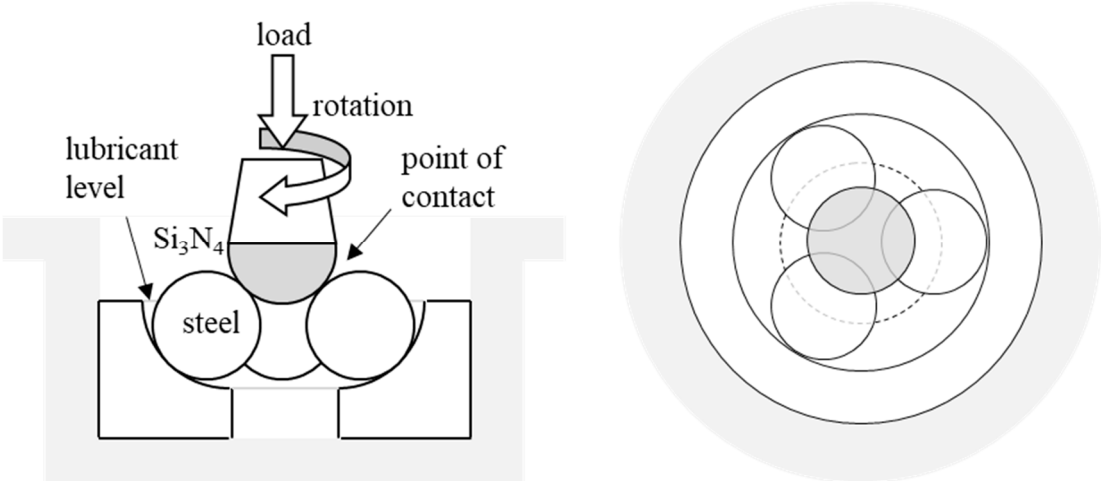

Figure 2. Loading and ball configuration in the four-ball tester. The point of contact was 1.96 mm above the lubricant level.

RCF tests were conducted in accordance with the IP-300 standard. The normal load at the point of contact (P_c) was calculated with the equation as follows:

$$P_c = \frac{P_m}{3cos\varphi}, \quad (1)$$

where P_m was the applied machine load and φ was 40.56° for the loading configuration in the tester. The machine load was 2200 N, which corresponded to a contact stress of approximately 7 GPa at the point of contact. The upper ball was silicon nitride with varied roughness. The three lower planetary balls and the race were AISI 52100. The point of contact was 1.96 mm above the surface of the lubricant and, as such, the lubricant did not flood the contact point. Instead, the rolling lower balls carried the lubricant into the contact point with the upper silicon nitride ball. Therefore, the reduced film thickness for a circular contact between spheres was used [22]. The film thickness ratio was calculated to be less than 1 (for all experiments).

The RCF tests were concluded when the first spalling of the upper silicon nitride ball was detected by the accelerometer. In the event of fatigue of any planetary lower balls, their fatigue life was recorded, and the fatigued planetary ball was replaced. The test would then continue with the previously used, undamaged upper ball. This step was repeated until eventual fatigue of the upper ball, at which point the test series was concluded. The race was also inspected intermittently for fatigue damage and replaced if necessary.

The applicability of the RCF life results using a four-ball tester to the real bearing applications has been addressed in the literature by multiplying them by a stress cycle factor. The stress cycle factor was calculated to be 2.25 for a four-ball tester that uses balls with a diameter of 12.7 mm [23]. In another experimental study, a factor of 6 was determined for the same four-ball tester [24]. Since this paper compares the RCF life of the top silicon nitride balls with various roughness parameters, the stress

cycle factor does not affect the comparison and is not considered in the representation of the fatigue life results.

3. Results

3.1. Data Analysis

The two-parameter Weibull distribution was chosen for the representation and analysis of fatigue test results, as described in detail in the literature [24–26]. The Weibull cumulative distribution function is typically represented as follows:

$$F(x) = 1 - e^{\left[-\left(\frac{x}{\alpha}\right)^{\beta}\right]} \tag{2}$$

where α is the scale parameter, β is the shape parameter, and x refers to the number of cycles to failure. The scale parameter, also called the characteristic life, is the life that 63.2% of tested samples attain before failure, while the shape parameter gives an indication of the rate at which the tested samples achieve the failure criteria. The distribution function is converted to log–linear form by applying logarithms to both sides, yielding the following equation:

$$\ln\ \ln\left[\frac{1}{1 - \mathrm{F(x)}}\right] = \beta \ln \mathrm{x} - \beta \ln \alpha,\ \mathrm{x} > 0 \tag{3}$$

where the shape parameter β is the slope, while the term -βlnα represents the intercept in the plot of $\ln\ \ln\left[\frac{1}{1-\mathrm{F(x)}}\right]$ against ln x. An approximation for the failure probability F(x) is obtained using the median ranks method. $\mathrm{F_i(x)} = (i - 0.3)/(k + 0.4)$ represents the median rank values where *i* is the rank of each sample in ascending order of fatigue life and k is the number of samples tested. Since the Weibull cumulative distribution function yields the probability of failure, the reliability could be obtained by subtracting the probability of failure from the total probability of 1. From the reliability data, the L_{10} life for each sample type could then be predicted.

3.2. RCF Life and Probablity of Failure

The RCF life results of original-finish silicon nitride balls for sample A (labeled A-SN) are illustrated in Figure 3. The corresponding RCF life of AISI 52100 lower balls (labeled A-52100) rolling against the silicon nitride in sample A are shown in Figure 4. As shown, the number of data points for upper balls is significantly less than those for the lower balls, due to the more frequent failure of the lower balls. In these charts, $\ln\ \ln\left[\frac{1}{1-\mathrm{F(x)}}\right]$ is plotted against ln x, where F(x) is approximated by the median ranks and x is the life of each sample in cycles. The actual life data are highlighted on each graph, along with the Weibull best-fit regression data. The linear (Weibull) line connects the Weibull best-fit regression data.

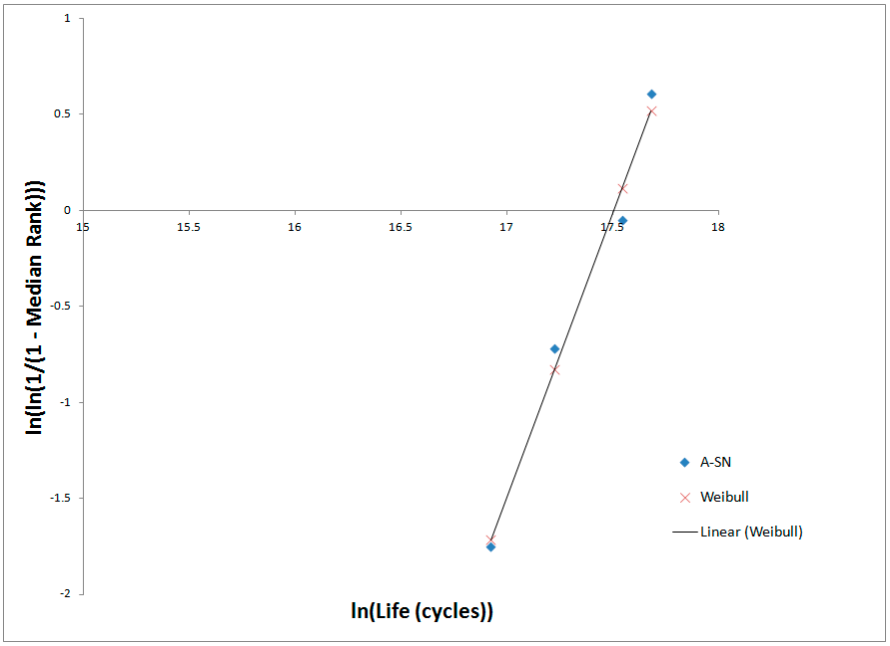

Figure 3. Rolling contact fatigue (RCF) life of original-finish Si_3N_4 upper balls (sample A).

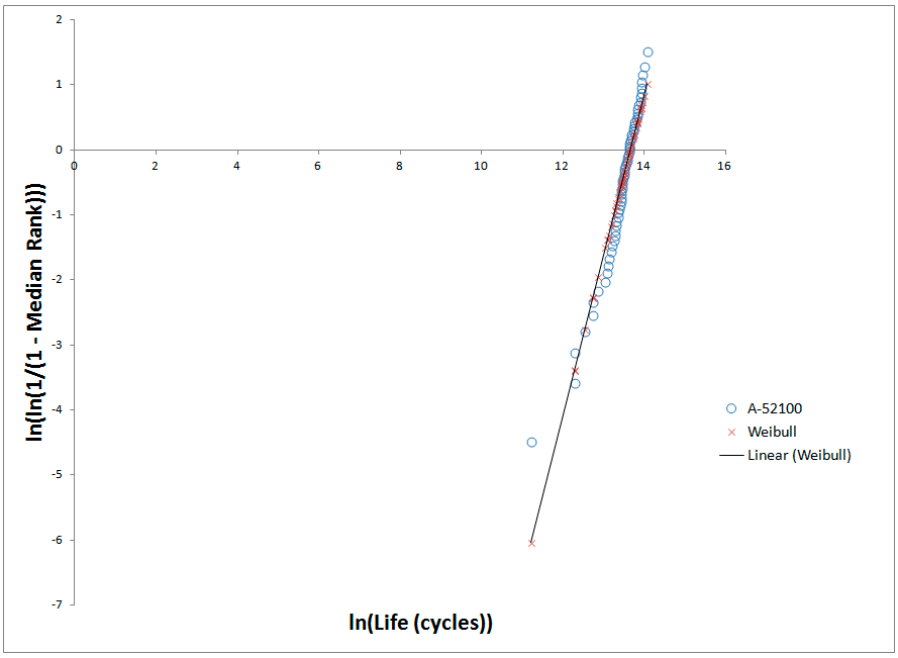

Figure 4. RCF life of 52100 lower balls against sample A.

Figure 5 shows the reliability of silicon nitride in samples A through F (labeled A-SN to F-SN) versus fatigue life. Here, reliability refers to the sample reliability, or the probability that a sample would survive a given number of cycles under the set loading conditions. The L_{10} life, the life at which 90% of samples survive, was calculated from the reliability data. Figure 6 exhibits the L_{10} life against the peak-to-valley roughness. As the peak-to-valley roughness increases, the L_{10} life decreases for every tested sample. In Figure 7, the L_{10} life is compared with R_a and the results indicate that the average roughness does not consistently correlate with the L_{10} life for every single roughness data point. For two instances where there were increases in the average roughness, the corresponding

life did not decrease. A similar plot was obtained when L_{10} life was compared with the root mean square R_q.

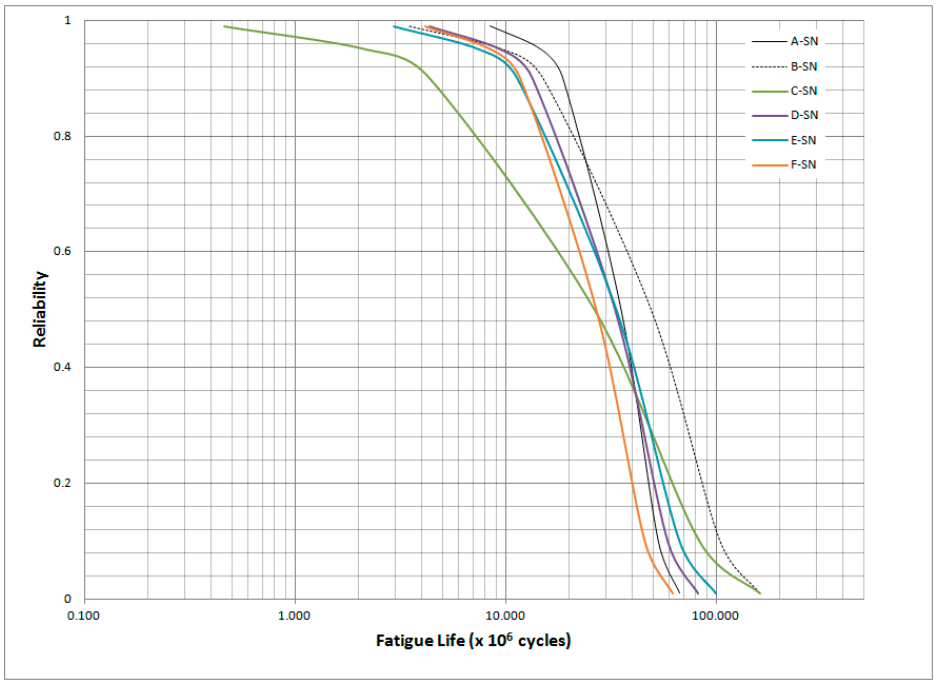

Figure 5. Fatigue life versus reliability for Si_3N_4 upper balls in hybrid configurations with AISI 52100 steel lower balls.

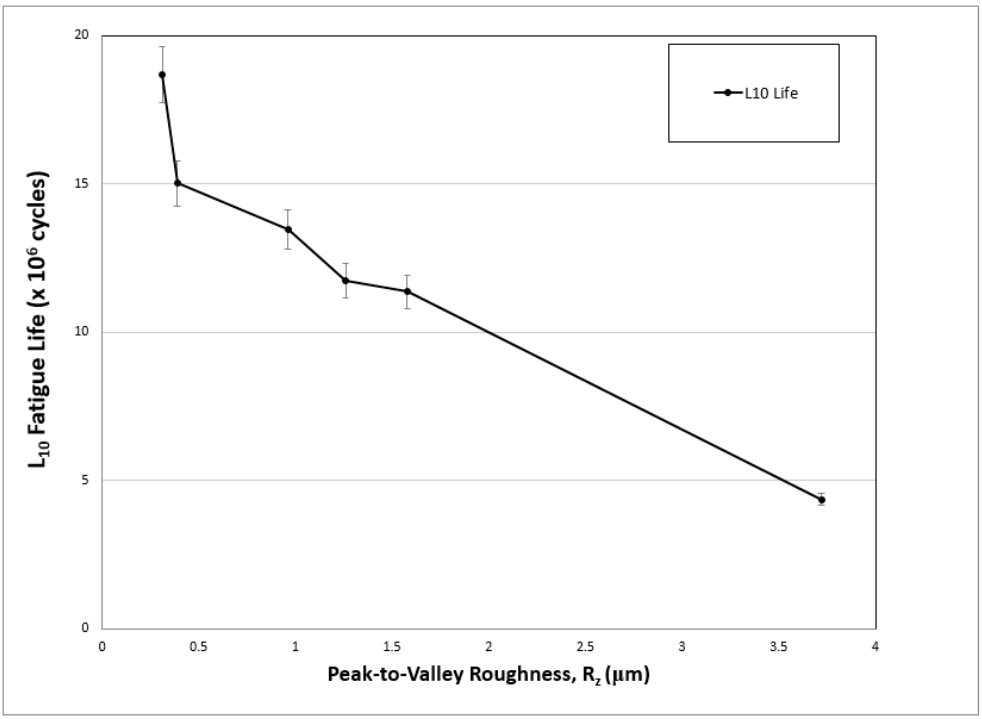

Figure 6. Variation of L_{10} life with R_z for Si_3N_4 upper balls.

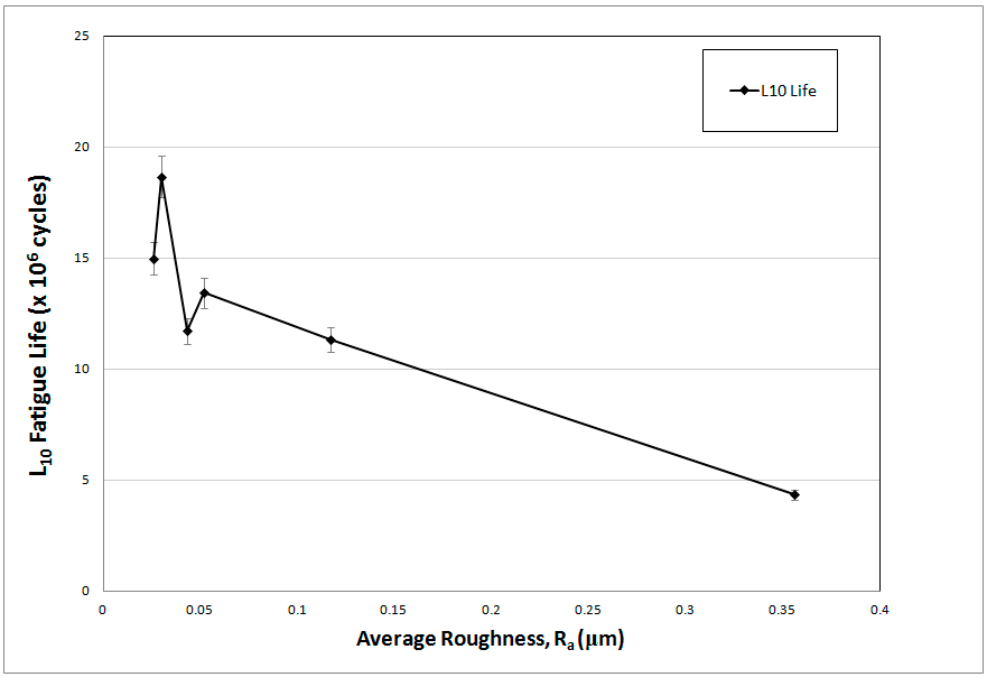

Figure 7. Variation of L_{10} life with R_a for Si_3N_4 upper balls.

The fatigue of silicon nitride balls was defined with the formation of the first spall, which was detected by a piezoelectric accelerometer. In Figure 8, the spalling of silicon nitride sample A (R_z = 0.312 m) is shown. The spall area is roughly 250 × 350 µm^2. The wear track also shows micropitting visible around the spalled region. The size of micropits is in the range of a few microns to a few ten microns. The micropits are randomly scattered on the wear track. The lower part of the image is the untested area outside the wear track with no micropitting.

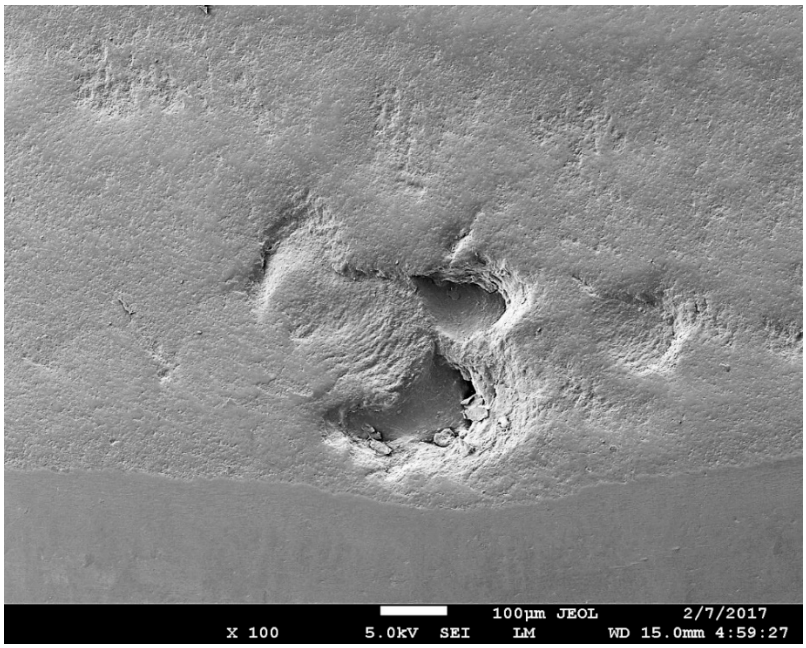

Figure 8. Spalling in Si_3N_4 upper ball sample A (R_z = 0.312 m). Micropitting of the wear track around the spalled area is mild.

The size of the first fatigued spall was increased for rougher surfaces. For instance, in silicon nitride sample E (R_z = 1.578 m), the spall area was 450 × 700 μm^2. Also, micropitting and macropitting areas were present around the spall, as shown in Figure 9, with a higher frequency of occurrence beyond the trailing edge of the spall. Within the spall, propagated cracks on various walls, i.e., side and trailing edge walls, and large propagated cracks at the trailing edge, were present. For silicon nitride sample E (R_z = 3.720 m), the fist spall area was 600 × 950 μm^2, as shown in Figure 10. Severe micropitting and macropitting on the wear track beyond the trailing edge of the spall was observed. Also, large cracks on the trailing edge wall of the spall are shown in Figure 10c. The cracks on the side wall of the spall are shorter in length than those on the trailing edge wall as shown in Figure 10d.

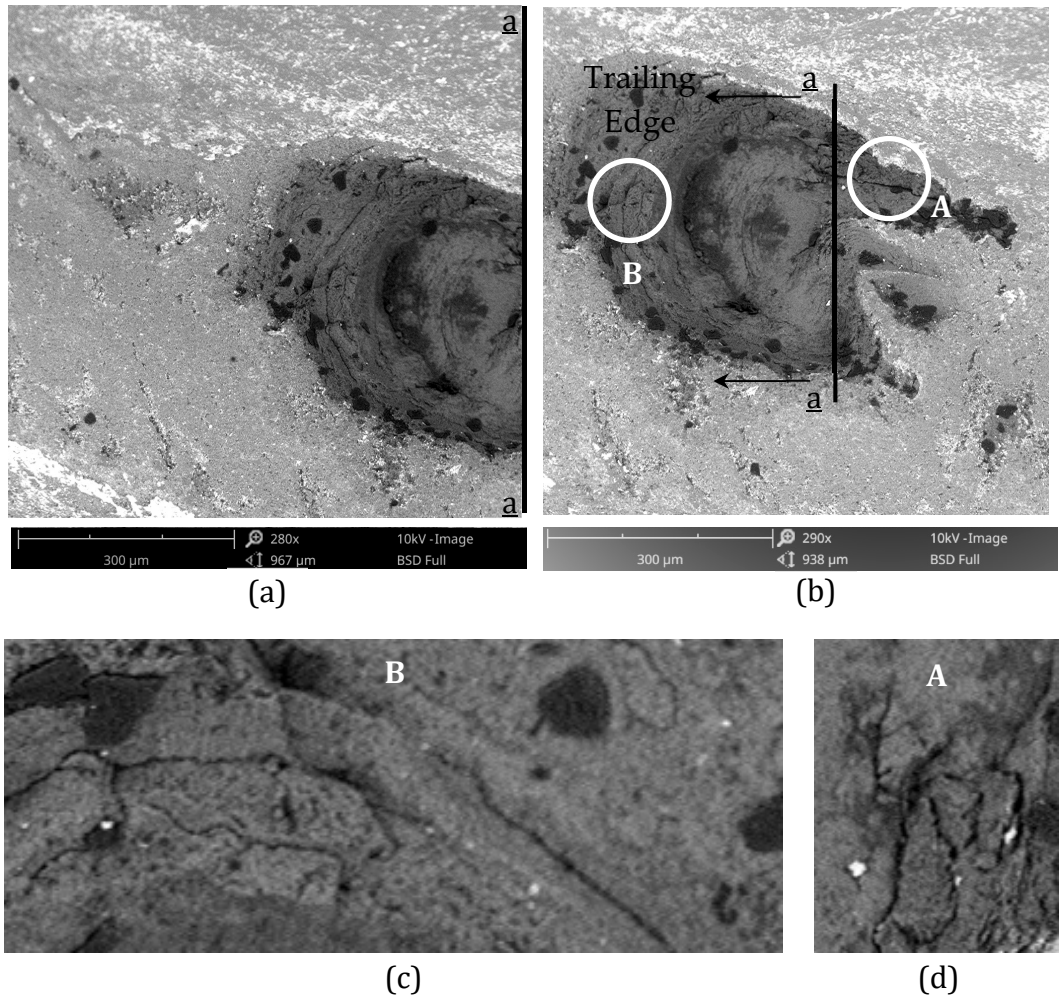

Figure 9. In sample E with R_z = 1.578 m, (**a**) micropitting and macropitting on the trailing edge of the spall, (**b**) spalling in Si_3N_4 upper ball, (**c**) long cracks in the spall at the trailing edge, and (**d**) cracks in the spall on the side.

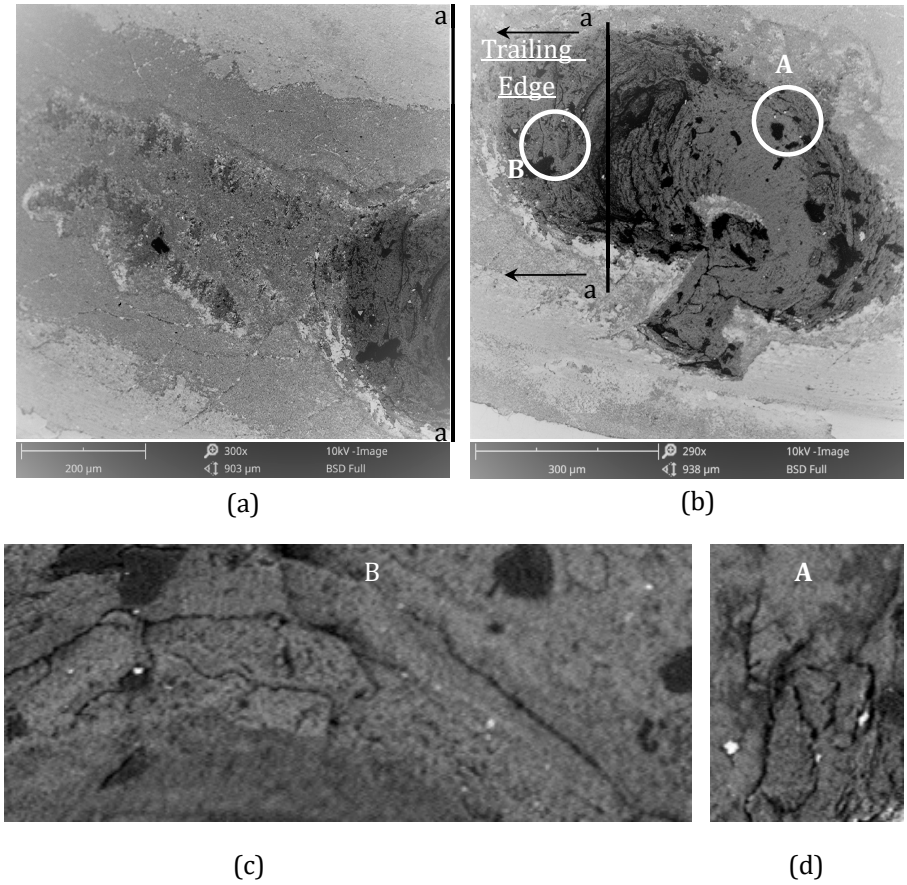

Figure 10. In samples F with R_z = 3.720 m, (**a**) severe micropitting and macropitting on the trailing edge of the spall, (**b**) spalling in Si_3N_4 upper ball Sample F, (**c**) long cracks in the spall at the trailing edge, and (**d**) cracks in the spall on the side.

4. Discussion

4.1. Role of Peak-to-Valley Roughness in Fatigue

The peak-to-valley roughness R_z, which was calculated by averaging the measured vertical distance from the highest peak to the lowest valley within five sampling lengths, contains information about the extreme features that affect the surface-initiated RCF life. As the experimental results presented in Figure 6 suggest, the rolling contact fatigue of silicon nitride decreased as the peak-to-valley roughness decreased, in a synchronized manner. This synchronized correlation was not established with other roughness parameters, such as R_a and R_q, which represent averages of all peaks and valleys of the roughness profile over the entire measurement length. In these roughness parameters, the extreme heights and valleys have no significant impact and, therefore, are not good representations of the RCF life of silicon nitride in conditions with marginal lubrication and significant asperity interactions, such as conditions encountered during the startup period of a bearing operation.

The microvalleys, which are better represented by the R_z value compared to the R_a and R_q values, have been shown to be the initiation sites for micropits in as-ground gears during contact fatigue. Also, the micropeaks that create localized high contact stresses on contacting surfaces can initiate microcracks leading to micropits in the mating surface under micro elastohydrodynamic lubrication (EHL) conditions [14,27]. The rolling track of silicon nitride balls E (R_z = 1.578 m) and F (R_z = 3.720 m) showed that micropits were created at the edge of polishing marks, as shown in Figure 11. The results are consistent with the notion that the initiation and growth of micropits from the notch-like microvalleys contribute to micropitting under cyclic loading [16].

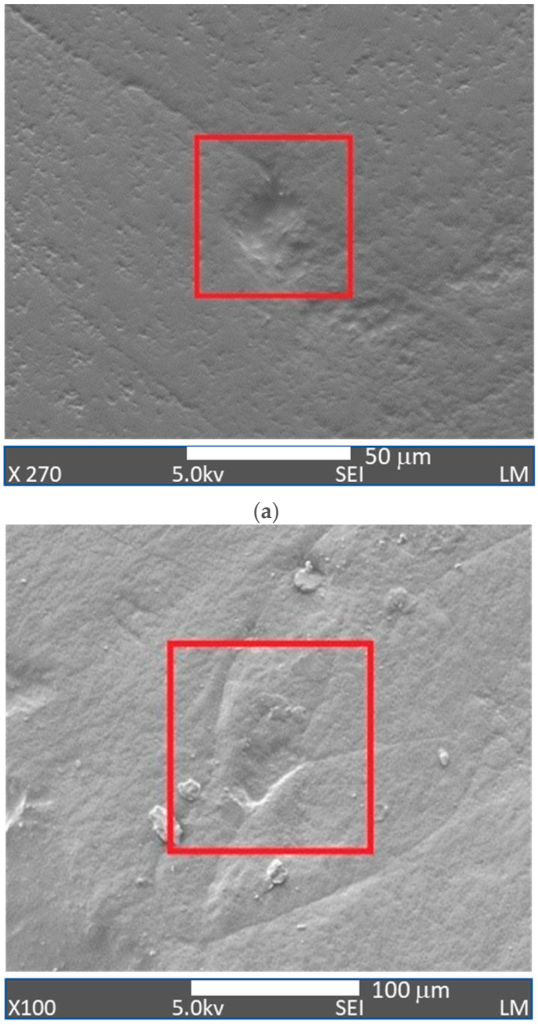

Figure 11. Micropitting at the end of polishing marks in (**a**) sample E (R_z = 1.578 m) and (**b**) sample F (R_z = 3.720 m).

The size of the first spall in silicon nitride ball samples increased as the roughness of the surface increased. Also, the spall region in rougher surfaces exhibited longer cracks at the trailing edge wall of the spall. As the literature suggests, as the ball moves through the spall length, it partially impacts the spall trailing edge as it climbs onto the intact rolling track. The impact creates stresses additional to the contact stresses and results in severe crack propagation and fatigue of the trailing edge wall. As a result, the spall is propagated and enlarged in the circumferential direction of the trailing edge [28]. The extensive micropitting and macropitting of the rolling track beyond the trailing edge, as shown in Figures 9a and 10a for samples E (R_z = 1.578 m) and F (R_z = 3.720 m), may be explained in terms of the instability of the ball as it moves through the spall. The movement involves unloading of the ball and the associated vibration and impact on the trailing edge of the spall, which can be extended to the regions right beyond the trailing edge.

4.2. State of Lubrication and Reduced Film Thickness

Since the point of contact between the upper and lower balls in the four-ball test setup was slightly above the level of the lubricant pool, the lubrication was not flooded. The lubricant was provided to the contact point by rolling of the lower balls in the pool that carried it to the contact point. In such situations, the "reduced" film thickness was calculated based on a formula in the literature [7].

The calculated central film thickness is shown in Table 3. The value of λ indicates marginal lubrication and significant asperity contact between surfaces.

Table 3. Film thickness ratio (λ).

Sample ID	λ (EHL "Reduced" Film Thickness)
A	1.06
B	0.99
C	0.57
D	0.46
E	0.37
F	0.16

The low lambda (λ) values associated with "reduced" film thickness in this investigation resulted in a shortened fatigue failure life of silicon nitride by nearly one order of magnitude compared to other studies with similar materials, loading, and speed conditions in the central film thickness calculations [2]. Nevertheless, the comparative assessment of the role of roughness parameters on the RCF life is not affected by the state of marginal lubrication in this study.

5. Conclusions

Experimental results show that the L_{10} RCF life of Si_3N_4 rolling elements against AISI 52100 steel under lubricated conditions decreases as the peak-to-valley roughness R_z of the surface increases. Although the same general trend of decreasing RCF life with increasing arithmetic mean roughness R_a was observed, the correlation between the RCF life and R_a was not synchronized. In two cases, the rolling contact fatigue life did not decrease as the arithmetic mean roughnesses increased. Rougher silicon nitride balls also experienced larger spalled regions. Also, in rougher surfaces, a region with significant micropitting at the trailing edge of the spall was observed. Additionally, the spalled region of rougher surfaces contained larger and more frequent propagated cracks at the trailing edge wall.

Author Contributions: Supervision, methodology, writing- original draft preparation, M.M.; Investigation, writing- review and editing K.A.S., K.K.B. and S.T.S.; Project administration, conceptualization, funding acquisition, J.H.B.

Funding: This work was supported by The Boeing Corporation under contract TBC-HU—GTA-1 (RA-8).

Acknowledgments: The authors acknowledge James Griffin of Howard Nanoscience Facility (HNF) for his assistance in materials characterization.

Conflicts of Interest: The authors declare no conflict of interest.

References

1. Wang, L.; Snidle, R.W.; Gu, L. Rolling contact silicon nitride bearing technology: A review of recent research. *Wear* **2000**, *246*, 159–173. [CrossRef]
2. Bhandhubanyong, P.; Akhadejdamrong, T. Forming of silicon nitride by the HIP process. *J. Mater. Process. Technol.* **1997**, *63*, 277–280. [CrossRef]
3. Ziegler, A.; Kisielowski, C.; Ritchie, R.O. Imaging of the crystal structure of silicon nitride at 0.8 Angstrom resolution. *Acta Mater.* **2002**, *50*, 565–574. [CrossRef]
4. Hadfield, M.; Stolarski, T.A. The effect of the test machine on the failure mode in lubricated rolling contact of silicon nitride. *Tribol. Int.* **1995**, *28*, 377–382. [CrossRef]
5. Polonsky, I.A.; Chang, T.P.; Keer, L.M.; Sproul, W.D. An analysis of the effect of hard coatings on near-surface rolling contact fatigue initiation induced by surface roughness. *Wear* **1997**, *208*, 204–219. [CrossRef]
6. Miller, G.R.; Keer, L.M.; Cheng, H.S. On the mechanics of fatigue crack growth due to contact loading. *Proc. R. Soc. Lond. A* **1985**, *397*, 197–209. [CrossRef]
7. Mosleh, M.; Bradshaw, K.; Belk, J.H.; Waldrop, J.C., III. Fatigue failure of all-steel and steel-silicon nitride rolling ball combinations. *Wear* **2011**, *271*, 2471–2476. [CrossRef]

8. Ås, S.K.; Skallerud, B.; Tveiten, B.W. Surface roughness characterization for fatigue life predictions using finite element analysis. *Int. J. Fatigue* **2008**, *30*, 2200–2209. [CrossRef]
9. Westkaemper, E.; Hoffmeister, H.W. Function-oriented lapping and polishing of ceramic rolling elements through characterization of the workpiece surface. *CIRP Ann. Manuf. Technol.* **1996**, *45*, 529–532. [CrossRef]
10. Effner, U.; Woydt, M. Importance of machining on tribology of lubricated slip-rolling contacts of Si_3N_4, SiC, Si_3N_4–TiN and ZrO_2. *Wear* **1998**, *216*, 123–130. [CrossRef]
11. Westkaemper, E.; Hoffmeister, H.W. Function-oriented surface characterization of lapped and polished ceramic rolling elements. In Proceedings of the 7th International Conference on Metrology and Properties of Engineering Surfaces, Gothenburg, Sweden, 2–4 April 1997; pp. 432–443.
12. Li, S.; Kahraman, A. Micro-pitting fatigue lives of lubricated point contacts: Experiments and model validation. *Int. J. Fatigue* **2013**, *48*, 9–18. [CrossRef]
13. Li, S.; Kahraman, A.; Klein, M. A fatigue model for spur gear contacts operating under mixed elastohydrodynamic lubrication conditions. *ASME J. Mech. Des.* **2012**, *134*, 11. [CrossRef]
14. Britton, R.D.; Elcoate, C.D.; Alanou, M.P.; Evans, H.P.; Snidle, R.W. Effect of surface finish on gear tooth friction. *ASME J. Tribol.* **2000**, *122*, 354–360. [CrossRef]
15. Batista, A.C.; Dias, A.M.; Lebrun, J.L.; Le Flour, J.C.; Inglebert, G. Contact fatigue of automotive gears: Evolution and effects of residual stresses introduced by surface treatments. *Fatigue Fract. Eng. Mater. Struct.* **2000**, *23*, 217–228. [CrossRef]
16. Moorthy, V.; Shaw, B.A. An observation on the initiation of micro-pitting damage in as-ground and coated gears during contact fatigue. *Wear* **2013**, *297*, 878–884. [CrossRef]
17. Kanga, J.; Hadfielda, M.; Cundillb, R.T. Rolling contact fatigue performance of HIPed Si_3N_4 with different surface roughness. *Ceram. Int.* **2001**, *27*, 781–794. [CrossRef]
18. Lv, B.H.; Chen, L.N.; Zhao, P.; Chang, M. Study on Fixed Abrasive Lapping Technology for Ceramic Balls. *Mater. Sci. Forum.* **2006**, *532*, 460–463. [CrossRef]
19. Yuan, J.L.; Lü, B.H.; Lin, X.; Zhang, L.B.; Ji, S.M. Research on abrasives in the chemical–mechanical polishing process for silicon nitride balls. *J. Mater. Process. Technol.* **2002**, *129*, 171–175. [CrossRef]
20. Umehara, N.; Kirtane, T.; Gerlick, R.; Jain, V.K.; Komanduri, R. A new apparatus for finishing large size/large batch silicon nitride (Si_3N_4) balls for hybrid bearing applications by magnetic float polishing (MFP). *Int. J. Mach. Tools Manuf.* **2006**, *46*, 151–169. [CrossRef]
21. Hah, S.R.; Fischer, T.E. Tribochemical Polishing of Silicon Nitride. *J. Electrochem. Soc.* **1998**, *145*, 1708–1714. [CrossRef]
22. Zaretsky, E.V. *Bearing Elastohydrodynamic Lubrication: A Complex Calculation Made Simple*; NASA Technical Memorandum; NASA: Washington, DC, USA, 1990.
23. Tourret, R.; Wright, E.P. *Rolling Contact Fatigue: Performance Testing of Lubricants*; Heyden and Son LTD: London, UK, 1977.
24. Mosleh, M.; Bradshaw, K. Role of component configuration in evaluation of accelerated rolling contact fatigue of ball bearings. *Wear* **2011**, *271*, 2681–2686. [CrossRef]
25. Murthy, D.N.P.; Bulmerc, M.; Eccleston, J.A. Weibull model selection for reliability modeling. *Reliab. Eng. Syst. Saf.* **2004**, *86*, 257–267. [CrossRef]
26. Moltoft, J. Statistical analysis of data from electronic component life tests (A tutorial paper). *Act. Passiv. Electron. Compon.* **1987**, *12*, 259–279. [CrossRef]
27. Sadeghi, F.; Jalalahmadi, B.; Slack, T.S.; Raje, N.; Arakere, N.K. A review of rolling contact fatigue. *J. Tribol.* **2009**, *131*, 1–15. [CrossRef]
28. Arakere, N.K.; Branch, N.; Levesque, G.; Svendsen, V.; Forster, N.H. Rolling Contact Fatigue Life and Spall Propagation of AISI M50, M50NiL, and AISI 52100, Part II: Stress Modeling. *Tribol. Trans.* **2009**, *53*, 42–51. [CrossRef]